NANO LETTERS

LETTER

pubs.acs.org/NanoLett

Surface Plasmon Resonances in Strongly Coupled Gold Nanosphere Chains from Monomer to Hexamer

Steven J. Barrow,[†] Alison M. Funston,[‡] Daniel E. Gómez,[§] Tim J. Davis,[∥] and Paul Mulvaney*[,†]

[†]School of Chemistry and Bio21 Institute, The University of Melbourne, Parkville, Victoria, 3010, Australia

[‡]School of Chemistry, Monash University, Clayton, Victoria, 3800, Australia

[§]School of Physics, The University of Melbourne, Parkville, Victoria, 3010, Australia

[∥]Division of Materials Science and Engineering, CSIRO, Clayton, Victoria, 3169, Australia

Supporting Information

ABSTRACT: We present experimental data on the light scattering properties of linear chains of gold nanoparticles with up to six nanoparticles and an interparticle spacing of 1 nm. A red shift of the surface plasmon resonance with increasing chain length is observed. An exponential model applied to the experimental data allows determination of an asymptotic maximum resonance at a chain length of 10−12 particles. The optical data are compared with analytical and numerical calculation methods (EEM and BEM).

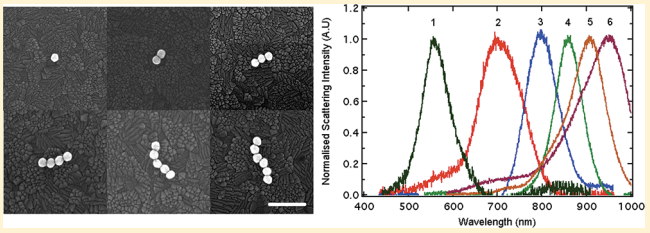

KEYWORDS: Surface plasmon, waveguide, nanoparticle, coupling, DNA, assembly

There is growing interest in the propagation of light in metal nanoparticle assemblies because of the potential to create optical devices smaller than the wavelength of light. The ability of metal nanoparticle chains, with an interparticle separation less than approximately 2.5 times the particle diameter, to accommodate the propagation of light arises as a result of near-field interactions between nanoparticles.[1−4,17] These are due to the overlap of the electromagnetic fields of the particles and could be exploited to allow the integration of nanoscale electronics with micrometer scale photonic systems.[5] This, along with guiding electromagnetic energy below the diffraction limit of light, cannot be achieved with current conventional photonic devices or waveguides.

Most attempts at creating linear chains of metal nanoparticles have involved top-down lithographic approaches.[2,6,7] One key limitation of these fabrication methods is that it is difficult to obtain small separations (<10 nm) and curvatures.[8] On the basis of the more efficient waveguiding observed in single crystalline nanowires compared to their noncrystalline counterparts,[9−11] it is possible that linear arrays of single nanocrystals are able to act as a waveguide much more efficiently than noncrystalline structures. However, the arrangement of single-crystal particles into the required linear arrays is nontrivial and remains a fundamental challenge for the field. Self-assembly techniques are now becoming robust enough to start producing structures on the nanoscale that can be used to test theoretical models. In parallel, methods for single particle spectroscopy have also been developed such that particle size and shape can be compared to the scattering spectra of single particles.[12−16] The combination of self-assembly techniques and single particle spectroscopy may be used to elucidate the effects of particle interactions in multiparticle nanostructures on the optical properties of the assembly.

The optical properties of metal nanoparticle chains have been predicted to depend not only on the nanoparticle material, size, and shape but also on the interparticle spacing and the number of coupled nanoparticles within a given chain,[5,7,17−19] a prediction that has been upheld by far-field observations on lithographically fabricated structures.[2,7,20]

The dispersion relation for wave propagation along nanoparticle chains with different compositions, nanoparticle sizes, and interparticle separations has been calculated by approximating the response of the particles as point dipoles,[19,20] with some calculations also taking into account next-nearest neighbor interactions.[19,20] More recently it has become clear that the inclusion of retardation and radiative damping in the calculations is important.[18,21,22] However, theoretical modeling of nanoparticle chains at small interparticle separation is challenging as the contribution of multipolar modes increases and the effect of next-nearest neighbor interactions at these small separations is unknown. Furthermore, at very small interparticle separations, quantum mechanical effects can become significant.[23]

While nanoparticle chains have been extensively examined theoretically, experimentally there have been relatively few investigations of linear nanoparticle arrays, especially for linear arrays of discrete nanocrystals, due, at least in part, to the difficulty of their assembly. In this paper we investigate the optical properties of gold nanoparticles self-assembled into chains of differing length (one to six particles) by directly correlating their spectral response to their structural properties. We measure the spectral

Received: June 21, 2011
Revised: August 24, 2011
Published: August 31, 2011

ACS Publications © 2011 American Chemical Society

Figure 1. SEM images of self-assembled nanoparticle chains. Mean diameter of gold particles is 64 nm. Interparticle spacings are estimated at 1 nm. Scale bar = 250 nm.

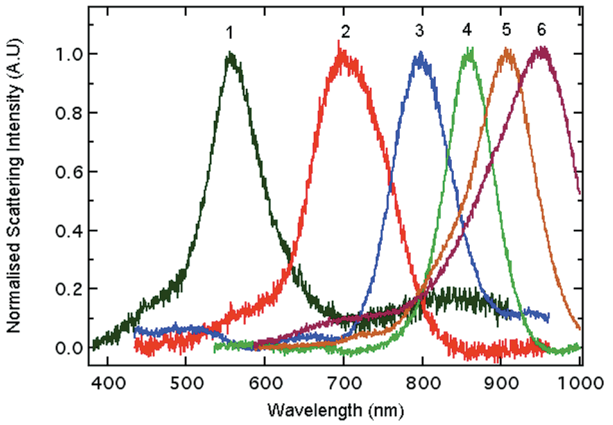

Figure 2. Normalized spectra of the nanoparticle chains in Figure 1. Spectra were collected in air on an ITO coated glass substrate. Spectra are numerically labeled according to chain length.

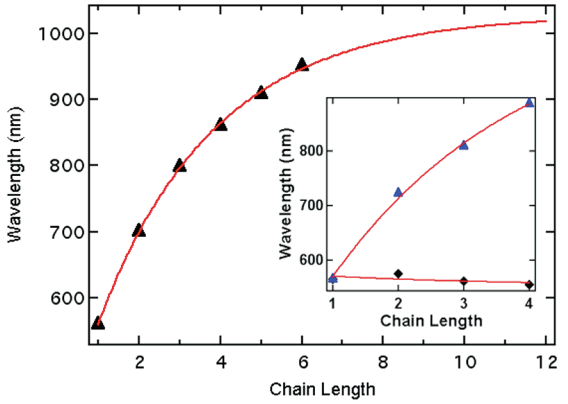

Figure 3. Maximum wavelength of longitudinal plasmon band plotted against number of particles in the given nanoparticle chain. Spectra were taken in air on an ITO coated glass substrate. Data points were obtained using a Lorentzian fit to the spectral data in Figure 2. Inset shows a plot of both the longitudinal (blue solid triangle) and transverse (black solid diamond) bands with increasing nanochain length. Measurements were taken in air on ITO substrates. Exponential fits are shown for each set of data (red lines) with the exponent fixed to have magnitude equivalent to that determined for the longitudinal mode, but with opposite sign, for the transverse bands to maintain an exponential fit.

response of one of the nanochains to polarized light and identified the plasmon resonance of the chain as a collective longitudinal mode. We show that higher-order modes and retardation must be included in order to quantitatively reproduce the experimentally observed plasmon resonances.

Spherical gold nanoparticles were prepared using the seed mediated wet chemical synthesis developed by Rodriguez-Fernandez et al.[24] Briefly, citrate seeds were prepared by bringing 100 mL of aqueous 0.25 mM chloroauric acid ($HAuCl_4$) to boiling temperature. Seed growth was initiated by the addition of 3.5 mL of aqueous 1 wt % sodium citrate solution. A deep red color after 20 min of boiling indicate the presence of gold nanoparticle seeds. Growth solutions were then prepared by adding 1 mL of a 1 wt % aqueous solution of $HAuCl_4$ to 88 mL of 0.015 M cetyltrimethylammonium bromide (CTAB). One milliliter of 0.05 M ascorbic acid was then added. Finally 10 mL of seed solution was added to initiate growth of the seeds. Subsequent growth steps were used to obtain a mean particle diameter of 64 nm. The nanoparticles were assembled using thiolated single strand oligonucleotides via a method adapted from the work of Yao et al.[25] Thiolated oligonucleotide strands (purchased from Geneworks) were reduced with tris(2-carboxyethyl)phosphine hydrochloride (TCEP) and added to nanoparticle solutions in a ratio of roughly 100 DNA strands per gold particle. Microliter volumes of nanoparticles with conjugate oligonucleotide strands were then mixed together. Assembly was initiated by adding a PBS buffer to the mixed nanoparticles. After the assembly had proceeded for approximately 5 min, the assembled particles were coated onto cleaned ITO coated glass slides for scanning electron microscopy (SEM) and darkfield microscopy. The nanoparticles within the chain are capped under these conditions with a mixture of the CTAB surfactant and DNA. As is it not possible to produce only linear chains via this method, many aggregates and nonlinear structures were evident in assembled samples. We selectively chose chain assemblies for analysis via the SEM/FIB-DFM correlation method. Nanochains of varying lengths were obtained by varying assembly times.

Refractive index experiments were performed using samples on ITO coated glass slides, and spectra were taken either in air or in dibromomethane. Nanoparticle samples were imaged using an xT Nova Nanolab SEM, and the substrate was etched using a focused ion beam (FIB) to allow for pattern matching when viewing samples under a darkfield microscope.[16] Scattering spectra were collected using a Nikon Eclipse TE-2000 coupled with a darkfield condenser, with a Nikon Plan Fluor ELWD objective and focused onto a MicroSpec 2150i imaging spectrometer coupled with a TE-cooled PIXIS 1024 ACTON Princeton Instruments CCD camera. Polarized scattering spectra were collected using a polarizer (LPVIS 100, Thorlabs) placed in the incident light path.

Figure 1 shows SEM images of the nanoparticle chains obtained via DNA assembly. The samples vary from single gold nanoparticles through to a chain six particles in length, each comprised of gold nanoparticles that are on average 64 nm in diameter. The oligonucleotides were selected to yield interparticle spacings of 5−6 nm. However the observed spacings were usually much less due to the large van der Waals interaction between these large gold nanoparticles. From the SEM images of the chains, we estimate the spacing as approximately 1 nm. This is an upper limit as the resolution of the FEG SEM is 1 nm. The

dx.doi.org/10.1021/nl202080a |*Nano Lett.* 2011, 11, 4180–4187

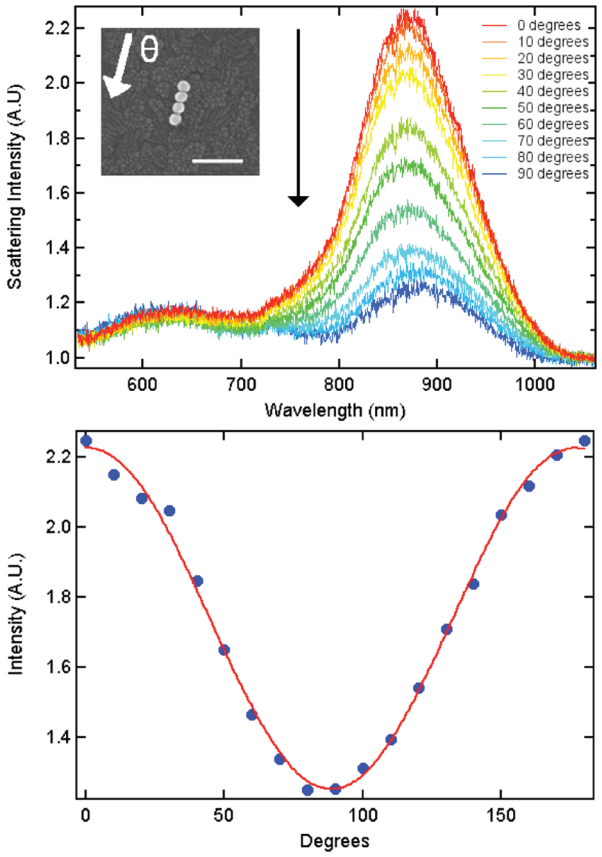

Figure 4. (Top) Four nanoparticle chain spectra at different polarizations. Inset shows an SEM image of the nanochain. The polarizer angle compared to the position of the four particle nanochain was known by using the FIB marks on the substrate as a reference. The 0° angle has been indicated on the inset SEM micrograph. The gold nanoparticles used were 64 nm in diameter and spectra were collected on an ITO coated glass substrate in air. The scale bar in the inset is 250 nm. (Bottom) Scattering intensity of the longitudinal plasmon band (870 nm) of a four particle chain resonance versus polarizer angle.

surfactant molecules (the majority of which are CTAB) coating the gold nanospheres are 1.0−1.5 nm long, so complete interdigitation of the surfactant molecules would also lead to a particle spacing in the order of 1 nm and is consistent with our previous work.[26,27] The scattering spectra obtained for the nanoparticle chains of Figure 1 are shown in Figure 2, the data for the longitudinal plasmon resonance maxima are given in Table 3 of the Supporting Information. As the nanoparticle chain length increases from one to six particles, the wavelength of the plasmon resonance with largest scattering intensity red shifts significantly. The observed red shift progressively decreases with chain length and begins to plateau. This resonance is identified as a longitudinal coupling mode along the length of the nanoparticle chain, and this is borne out by its response to polarized excitation light (see below) and is also consistent with the plasmon hybridization model[28,29] and dispersion relation calculations.[20] A second, less intense resonance was observed at wavelengths ranging from 500 to 600 nm (see inset of Figure 3), which is attributed to the mode transverse to the axis of the nanoparticle chain. This resonance blue shifted only slightly with an increase in the chain length. The experimentally observed red shift of the longitudinal coupled mode as a function of nanoparticle chain length was fitted to the empirical formula

$$\lambda = \lambda_0 + (\lambda_\infty - \lambda_0)(1 - e^{-\tau/N}) \quad (1)$$

where λ_0 = 520 nm, the measured single particle surface plasmon wavelength on a substrate and in air (i.e., under the same experimental conditions as the nanoparticle chains), N is the chain length, τ is the fitted parameter, and λ_∞ is the predicted asymptotic wavelength of an infinitely long nanoparticle chain. In Figure 3 the observed relationship between the energy of the maximum plasmon absorption and chain length is plotted. The exponential fit gives τ = 2.89 and λ_∞ = 1028 nm, which occurs at a chain length of approximately 10−12 nanoparticles. Such an exponential trend is in accordance with the theoretical models of Maier et al.[7] and Fung et al.[19] and a plateau at a chain length of approximately 10 has been theoretically predicted for nanoparticle chains at small interparticle separations (<5 nm) using rigorous approaches.[5,18,30,31] Figure 4 shows the spectral response of a four-particle length nanochain when exposed to excitation light of varying polarizations. Spectra were taken at 10° increments of the polarizer and a plot of plasmon band intensity versus polarizer angle can also be seen in Figure 4. The spectra show a decrease in intensity as the polarization of the electric field is changed from parallel to the chain axis to perpendicular to the chain axis. Note that the orientation of the nanoparticle chain with respect to the incoming light vector is known, due to the use of orienting FIB etch marks.

For a perfectly linear chain exhibiting a dominant longitudinal plasmon resonance, it would be expected that, when the incident light is polarized perpendicular to the chain, no longitudinal resonance should be evident (the polarization discrimination of the optical filter used in these experiments in the range 600−1200 nm is >100000: 1). Although the four-particle chain is almost perfectly linear, the longitudinal resonance could not be completely removed from the spectra, even when rotating in 2° intervals around the point of lowest scattering. This was the case for all chains investigated (see for example the 5-particle chain in Figure 3 in the Supporting Information).

"Polarization" refers to the polarization density P, which is related to the incident electric field E by

$$P = \alpha E \quad (2)$$

E has a polarization, which refers to how it is aligned to a given reference coordinate system. For nanoparticles exhibiting disorder (i.e., variations in interparticle distances and orientations) in the direction of the incident field, the induced polarization in the particle chains and therefore the resultant plasmon mode is not parallel to the polarization of the incident field. In this case there is an anisotropy in the polarizability of the nanoparticle chain. Despite this, for longitudinal excitation, the effect of even 6.25% disorder (1 standard deviation) is predicted to have a marginal effect on induced dipole moments in nanoparticle chains for which the dipole approximation is valid.[32] A small degree of disorder in the particle size or shape for long arrays of nanoparticles has also been predicted to have minimal effect,[33] although this may be more prominent for short nanoparticle chains such as those described here. Therefore, despite the slight curvature observed in the longer nanpoarticle chains shown in Figure 1, the effect of disorder on the energy of the longitudinally coupled plasmon mode is expected to be minimal.

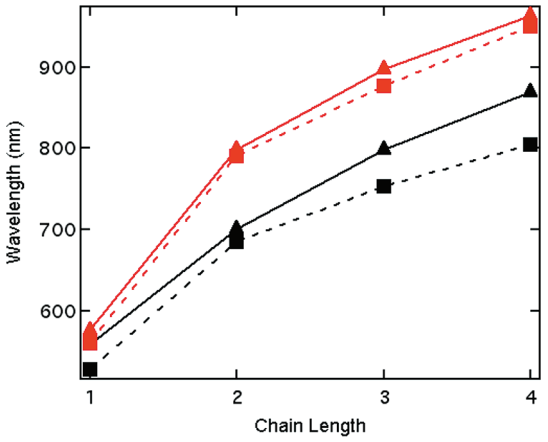

Figure 5. Plot of the experimental longitudinal plasmon wavelength versus chain length for nanochains in air (black solid triangle) and dibromomethane (red solid triangle) and predicted plasmon wavelengths using BEM in both air (black solid square, RI = 1.28) and dibromomethane (red solid square, RI = 1.54). Raw data are given in the Supporting Information.

The experimentally measured plasmon resonance energy of the nanoparticle chains may be used to gain insight into the waveguiding potential of infinitely long nanoparticle chains with the same nanoparticle size and interparticle separation as the systems synthesized here. The dispersion relation for wave propagation along nanoparticle chains with interparticle separation $\geq 1/2d$ (where d is the particle diameter) has been calculated approximating the response of the nanoparticles as point dipoles.[19,20] For these nanoparticle chains, consisting of relatively large nanoparticles (64 nm diameter) with very small interparticle separation, retardation, next-nearest neighbor effects, and the inclusion of higher order modes are expected to be important. However, some physical insight may be gained from relationships derived via calculation of the waveguiding dispersion relation when modeling the nanoparticles as point dipoles (i.e., within the electrostatic approximation).

In the far-field excitation geometry, all the particles in the chain are excited in phase and the change in energy of the chain's collective resonance mode compared to the localized plasmon resonance of a single, uncoupled particle is related to the $\mathbf{k} = 0$ modes of the dispersion relation. These energy differences can thus be used to estimate the attenuation length of propagating plasmon modes within the electrostatic approximation.[2,7,34] Extrapolating the red shift of the coupled longitudinal chain resonance to >12 spheres (i.e., to its plateau), 1028 nm (1.206 eV), it may be calculated that the bandwidth available for energy transport via the longitudinal mode in an infinite linear array of nanoparticles of the same size and interparticle separation, B_L is 1.974 eV ($B_L = 2|E_0 - E_L|$ where E_0 is the energy of the localized surface plasmon resonance of a single sphere, 565 nm (2.193 eV)) while the equivalent value for the transverse mode is 86 meV (where E_T is 553 nm (2.236 eV) from the inset of Figure 3). Using far-field measurements on single, isolated spheres allows the homogeneous line width of the plasmon resonance to be measured as $\Gamma = 367$ meV (average of two spheres). Note that for this system Γ is quite large due to the (relatively) large size of the spheres used. Thus, for transport of light via the longitudinal mode at the single particle resonance (2.193 eV), where it is predicted by the dipole approximation to be most efficient, according to $\alpha_L = \Gamma/(B_L d)$, the attenuation factor α_L is 2.9×10^6 m^{-1}, and the energy loss, $2\alpha_L$ is 5.7×10^6 m^{-1} or 3 dB per 175 nm. This represents a relatively small energy loss compared with other experimentally determined values.[2,7] While Γ is relatively large for this system it is more than compensated for by the extremely strong near-field interaction of the closely spaced nanoparticles. Note that these calculations do not take into account absorptive losses.

Given the limitations and obvious disadvantage that the point-dipole model used to derive the above relationships will break down for the structures synthesized here, it is pertinent to compare more rigorous calculations. More recent theoretical investigations into waveguiding within linear nanoparticle chains which include retardation have shown that for even moderately small nanoparticle chains dynamic effects are important[20,35] and that modes with energy below the light line are expected to be less lossy; thus, provided the longitudinal mode here is below the light line, the above calculation would overestimate the energy loss. In addition, contribution of higher order multipoles to the waveguiding modes in closely spaced systems have been theoretically investigated.[18,31] These calculations predict the emergence of low-loss subradiant modes which support the propagation of plasmons along the nanoparticle chain as the particle separation becomes smaller.[31] The subradiant modes are predicted to be higher energy than the lowest energy longitudinal mode, apparent as a shoulder/s on to the high energy side of the longitudinal mode for silver chains of >5 particles and for the system geometry investigated these lie below the light line. For gold nanoparticle chains these resonances might be expected to be broader, and it is possible these may appear as a broadening on the high-energy side of the longitudinal resonance of the coupled structure for chains $n > 5$. Inspection of the spectra in Figure 2 reveals a significant asymmetry of the longitudinal plasmon resonances for the five and six particle chains in support of this.

Figure 5 shows the longitudinal plasmon wavelengths of nanoparticle chains with lengths of one to four particles both in air (that is, at the ITO−air interface) and in dibromomethane ($n = 1.54$, the particles on the ITO substrate were immersed in the liquid) which closely matches the refractive index of the ITO-coated glass substrate.

To further investigate the physical nature of the modes observed, we employ the electrostatic eigenmode approximation (EEM).[36,37] Within this formulation, the surface plasmon resonances of nanoparticles are attributed to oscillating surface charge distributions $\sigma(\vec{\mathbf{r}})$. For an arbitrary array of N nanoparticles, these charge distributions can be written as a superposition of the "normal modes" of each particle of the ensemble

$$\sigma(\vec{\mathbf{r}}) = \sum_{\alpha=1}^{N} \sum_{j} a_\alpha^j \sigma_\alpha^j(\vec{\mathbf{r}}) \tag{3}$$

this collective or ensemble charge distribution satisfies an eigenvalue equation

$$\sigma(\vec{\mathbf{r}}) = \frac{\Lambda}{2\pi} \oint \sigma(\vec{\mathbf{r}}_q) \frac{(\vec{\mathbf{r}} - \vec{\mathbf{r}}_q)}{|r - r_q|^3} \hat{n} dS_q \tag{4}$$

where Λ are the eigenvalues which are related to the resonance wavelength (frequency) of the surface plasmon modes in the

dx.doi.org/10.1021/nl202080a |*Nano Lett.* 2011, 11, 4180–4187

coupled nanoparticles

$$\varepsilon_M(\lambda) = \varepsilon_b \frac{1 + \Lambda}{1 - \Lambda} \tag{5}$$

Here, λ is the peak wavelength of the surface plasmon resonance, $\varepsilon_M(\lambda)$ is the (wavelength dependent) permittivity of the metal, and ε_b that of the (uniform) background medium. For a single spherical nanoparticle $\Lambda = 3$ (dipolar mode) this equation reduces to the familiar resonance condition $\varepsilon_M(\lambda) = -2\varepsilon_b$ (the Fröhlich mode) We have previously shown that the eigenvalue eq 4 for a system of interacting particles can be written in terms of the noninteracting constituents, a procedure that results in an eigenvalue equation for the coefficients in eq 3[38]

$$\mathbb{K} \cdot \vec{\mathbf{a}} = \frac{2\pi}{\Lambda} \vec{\mathbf{a}} \tag{6}$$

The nontrivial solutions to this last equation are the roots of the characteristic equation: $\det\{(\mathbb{K} - 2\pi/\Lambda)\ 1\} = 0$. The off-diagonal elements of the matrix $\mathbb{K}$ describe the electrostatic interactions between the particles. As a starting point, one can assume that the leading term in the interaction is the dipole−dipole coupling and that, furthermore, only nearest-neighbor coupling is non-negligible. With these simplifications, the matrix $\mathbb{K}$ takes on the following general form, for a uniformly spaced linear chain containing N identical nanoparticles

$$\mathbb{K} \approx \begin{pmatrix} \frac{2\pi}{\gamma} & C & 0 & \cdots \\ C & \frac{2\pi}{\gamma} & C & \\ 0 & C & \frac{2\pi}{\gamma} & \\ \vdots & & & \ddots \end{pmatrix}_{N\times N} \tag{7}$$

where the diagonal elements contain the eigenvalues $\gamma = 3$ of the individual particles (spherical symmetry, dipole mode only). C is the dipole−dipole coupling constant which is given by the familiar expression

$$C \approx \frac{1}{d_{12}^3} (3(\mathbf{p}_1 \cdot \hat{\mathbf{d}}_{12})(\mathbf{p}_2 \cdot \hat{\mathbf{d}}_{12}) - \mathbf{p}_1 \cdot \mathbf{p}_2) \tag{8}$$

d_{12}, being the center to center distance between particles 1 and 2, and $\mathbf{p}$ the dipole moment. We can divide the elements of $\mathbb{K}$ by C and defining $x = 2\pi/\gamma C$, we get the following tridiagonal matrix

$$\begin{pmatrix} x & 1 & 0 & \cdots \\ 1 & x & 1 & \\ 0 & 1 & x & \\ \vdots & & & \ddots \end{pmatrix}_{N\times N} \tag{9}$$

The advantage of rewriting the coupling problem in terms of a tridiagonal matrix is that the eigenvalues and eigenvectors of such matrices have exact algebraic forms for any value of N.[39] For the matrix $\mathbb{K}$, the lowest energy eigenvalue is given by

$$\frac{1}{\Lambda_N} = \frac{1}{\gamma} + \frac{C}{\pi} \cos\left(\frac{\pi}{N + 1}\right) \tag{10}$$

corresponding to "hybridized" surface plasmon modes where all the dipoles are oriented in the same direction along the length of the particle chain. The first term in this equation depends on the eigenvalue γ of the noninteracting nanoparticles, (for spheres $\gamma = 3$ for the dipolar plasmon mode). The last term depends only on the number of particles in the linear chain (N) and the coupling constant C. For $N = 1$, the model correctly predicts that the eigenvalue of the coupling matrix is γ and, consequently, the surface plasmon frequency (or wavelength) corresponds to that of a single particle. This equation predicts, in agreement with our experimental observations, that in the limit where N approaches infinity, the surface plasmon resonance wavelength reaches an asymptotic value that is controlled by the geometry of the individual particles (through the parameter γ), the dielectric constant of the uniform surrounding medium (implicitly related as implied by eq 5), and the magnitude of coupling constant C

$$\varepsilon_M(\lambda_\infty) = \varepsilon_b \frac{1 + \gamma(C/\pi + 1)}{1 + \gamma(C/\pi - 1)} \tag{11}$$

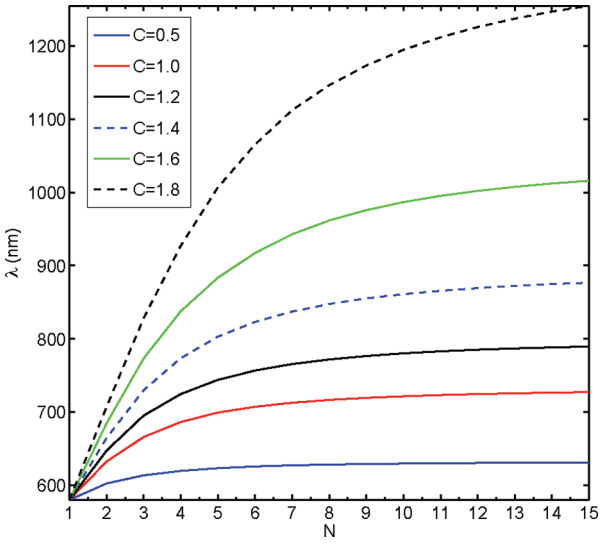

Figure 6. Plot of the surface plasmon resonance of linear chains embedded in a dielectric medium of refractive index $n = 2$ for different values of the nearest-neighbor coupling constant C, using eq 10.

In Figure 6 we show how this asymptotic limit changes with the value of C. Numerical calculations for a dimer of 64 nm diameter Au spheres with a spacing of 1 nm give a longitudinal dipole−dipole coupling constant $C_{dd} = 0.9957$ giving the results shown in Figure 7.

Clearly, the model underestimates the wavelengths of surface plasmon resonances of the chains. This is not surprising since at the short interparticle distances observed experimentally, the contributions to the coupling by higher order multipoles should be considered. If we include more than the dipolar plasmon mode to describe the interparticle coupling, the matrix shown in eq 7 increases in size and its symmetry is no longer tridiagonal. For each particle, the diagonal elements must include factors related to the wavelength of each plasmon mode (i.e., elements for the dipole $2\pi/3$, quadrupole $2\pi/5$, etc.[36]). The nondiagonal elements will consequently include additional interactions such as dipole−quadrupole, dipole−octupole, etc., which are not symmetric with respect to inversion (i.e., dipole−quadrupole coupling of particle 1 to 2 is not equivalent to quadrupole−dipole coupling of particle 2 to particle 1). However, one can use the partitioning method developed by Löwdin[41] to derive an

dx.doi.org/10.1021/nl202080a |Nano Lett. 2011, 11, 4180–4187

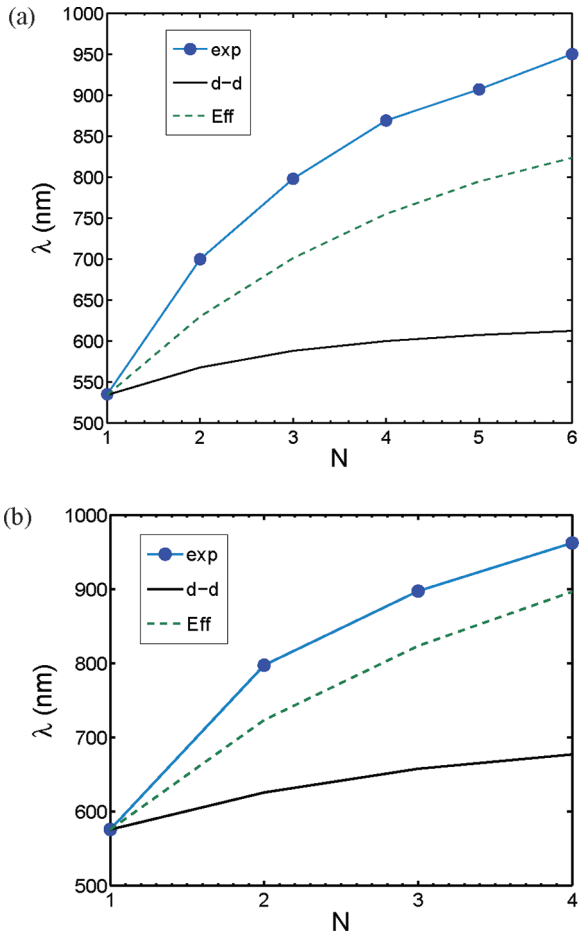

Figure 7. Plot of the surface plasmon resonance (nanometers) as a function of the number of particles, *N*, in a linear chain. (a) on glass in air and (b) in dibromomethane (index matching). For both of these, the experimental data are shown using the solid blue circles (with the points connected by a solid blue line) and labeled "exp"; the calculated response using the dipole−dipole model (corresponding to eq 8 using $\gamma = 3$ and $C = 0.9957$) is the solid black line, labeled d-d; the calculated response including corrections from higher-order multipolar coupling as discussed in the text is shown by the dashed green line and labeled "Eff". For (a), an effective medium dielectric constant for the surroundings with dielectric $\varepsilon_b = 1.562^2$ as reported previously,[40] while for (b) the essentially uniform background medium was taken to be $\varepsilon_b = 1.962^2$.

"effective" dipole−dipole coupling matrix (an *N* by *N* problem) that contains the perturbations caused by higher-order multipole interactions (details in the Supporting Information). With this partitioning, the coupling matrix takes on a form that is similar to that of eq 7, except that γ and *C* are replaced by "effective" values. With this approach, the resulting interaction matrix is tridiagonal and its eigenvalues are therefore those given in eq 10 but with the modified values of γ and *C*. Considering coupling up to the fourth multipolar mode gives $\gamma_{eff} = 2.3187$, a value that is lower than the ideal $\gamma = 3$ for a dipole and $C_{eff} = 1.3984$ a value higher than the dipole−dipole coupling constant (these values correspond to 64 nm spheres with 1 nm spacing). The predictions of this effective model, also shown in Figure 7, are in closer agreement to the experimental data. A better quantitative description of the data could be obtained by including more multipoles in the interparticle interaction (see Supporting Information). While it is expected that inclusion of interparticle coupling beyond the

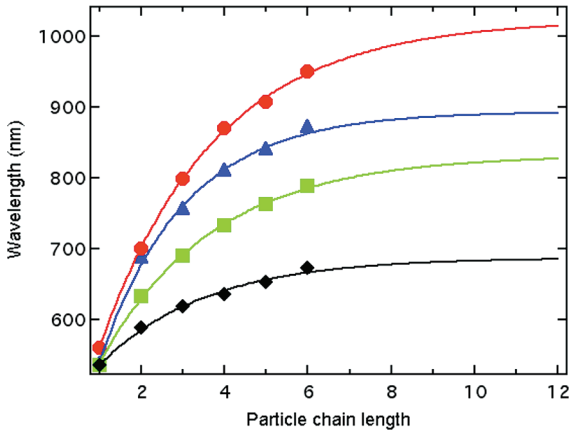

Figure 8. Calculated BEM models of nanoparticle chains along with the experimental data (red solid circle) from Figure 3. Chain lengths vary from one to six particles in length with spacings of 1 (blue solid triangle), 2 (green solid square), and 5 (black solid diamond) nm. Simulations involved 64 nm diameter gold nanoparticles in a medium with homogeneous refractive index of 1.28.

nearest neighbors will be required for a fully quantitative description of the data, the error introduced by neglecting these effects is small. Additionally, in these EEM calculations, no retardation effects were considered which are expected to contribute to the observed discrepancies, especially for longer chains.

In order to achieve more quantitative agreement, we performed boundary element method (BEM) calculations for nanoparticle chains consisting of one to six particles in length, using the program BEMAX developed by de Abajo.[42,43] The parameters utilized in these calculations are noted in the Supporting Information. The effect of nanoparticle spacing was also investigated by modeling these chains with spacings of 1, 2, and 5 nm. The energy of the plasmon resonance as calculated by BEM for different chain lengths are shown in Figure 8. As the interparticle separation decreases, the calculations tend toward the experimental results. The model neglects to take higher order coupling into account and therefore would not be expected to exactly predict the experimental data.[42,43] The BEM models, shown in Figure 8 exhibit the same exponential relationship between chain length and plasmon band as the experimentally determined results.

However, it can also be seen that changing the particle spacing drastically affects the rate at which the surface plasmon peak wavelengths reach the asymptotic ($N \rightarrow \infty$) value. Larger interparticle spacings result in the plateau of the exponential occurring at shorter chain lengths, consistent with a decreased interparticle coupling as predicted by our simple analytical model (see Figure 6 and eq 11). As the particle spacing is decreased for a given particle chain, the plasmon resonance red shifts as expected[8,18,19]

However, significant differences between experiment and theory remain. The inability of both the electrostatic eigenmode method (EEM) and the boundary element method (BEM) to quantitatively reproduce the data is a result of several factors. First, as inferred from the EEM, the short interparticle distances realized in our experiments imply strong coupling of a high number of multipolar modes. The results presented in Figure 7 were limited to a relatively small number of such multipoles and, in general, the EEM will asymptotically approach the experimental results as this number is increased. We have assumed in our

dx.doi.org/10.1021/nl202080a |*Nano Lett.* 2011, 11, 4180–4187

models that the nanoparticle chains form perfect straight lines and thus made assumptions regarding their nearest-neighbor coupling. However, as shown in our SEM images, some chains show a degree of curvature which is expected to introduce some "off-diagonal" disorder in the coupling matrix (within the EEM) and therefore alter the collective surface plasmon resonance. For the longest chain studied, the length of the resulting assembly is about 400 nm. At this size scale retardation effects must be considered, effects that were not included in our EEM model and thus contributed to the observed experiment−theory mismatch. A third point to consider is that in both of our models we have assumed the nanoparticle chains to be surrounded by an infinite and homogeneous (nonabsorbing) dielectric. Vernon et al.[44] and Knight et al.,[45] however, have demonstrated that interactions with the substrate will lead to significant spectral shifts. Finally, it is possible that at the interparticle separations of the chains measured here, quantum mechanical effects may become important and these are not considered by either the EEM or BEM.

In conclusion, the light scattering properties of self-assembled gold nanoparticle chains have been investigated and compared to both a semianalytical and a numerical model. It has been shown experimentally that the magnitude of the red shift of the plasmon resonance asymptotes to a finite value with increasing chain length and that the resonance peaks arise due to the presence of a single resonant mode. On the basis of the electrostatic eigenmode method, we have derived an analytical expression to describe the interparticle coupling in these chains, which explains most of the observed trends, in particular the asymptotic chain plasmon mode was found to depend on the interparticle coupling strength and the dielectric constant of the background medium. We have shown that both the BEM and EEM fail to reproduce quantitatively the plasmon resonances of the self-assembled gold nanoparticle chains. From our analysis of the coupling with the EEM, we found that the main shortcomings arise from our initial assumption of nearest-neighbor coupling and consideration of interparticle coupling of only a finite number of plasmonic multipolar modes. Both our experimental and theoretical results pave the way for a rational design of plasmonic assemblies.

■ ASSOCIATED CONTENT

Supporting Information. Additional details on next-nearest dipole−dipole coupling and effective dipole−dipole coupling, and boundary element method calculations, and a figure showing scattering spectra of a five-particle nanochain. This material is available free of charge via the Internet at http://pubs.acs.org.

■ AUTHOR INFORMATION

Corresponding Author

*E-mail: mulvaney@unimelb.edu.au.

■ ACKNOWLEDGMENT

This work was supported through Grant 100100117. The authors thank Sergey Rubanov of the Bio21 Electron Microscopy (EM) Unit for assistance with FIB/SEM. S.J.B. would like to thank the University of Melbourne for the Ernst and Grace Matthaei research scholarship. D.E.G. would like to thank the ARC for support (DP 110101767).

■ REFERENCES

(1) Maier, S. A.; Brongersma, M. L.; Kik, P. G.; Meltzer, S.; Requicha, A. A. G.; Atwater, H. A. *Adv. Mater.* **2001**, *13*, 1501–1505.
(2) Maier, S. A.; Kik, P. G.; Atwater, H. A.; Meltzer, S.; Harel, E.; Koel, B. E.; Requicha, A. A. G. *Nat. Mater.* **2003**, *2*, 229–232.
(3) Barnes, W. L.; Dereux, A.; Ebbesen, T. W. *Nature* **2003**, *424*, 824–830.
(4) Halas, N. J. *Nano Lett.* **2010**, *10*, 3816–3822.
(5) Sweatlock, L. A.; Maier, S. A.; Atwater, H. A.; Penninkhof, J. J.; Polman, A. *Phys. Rev. B* **2005**, *71*, 7.
(6) Hicks, E. M.; Zou, S. L.; Schatz, G. C.; Spears, K. G.; Van Duyne, R. P.; Gunnarsson, L.; Rindzevicius, T.; Kasemo, B.; Kall, M. *Nano Lett.* **2005**, *5*, 1065–1070.
(7) Maier, S. A.; Kik, P. G.; Atwater, H. A. *Appl. Phys. Lett.* **2002**, *81*, 1714–1716.
(8) Jain, P. K.; El-Sayed, M. A. *J. Phys. Chem. C* **2008**, *112*, 4954–4960.
(9) Maier, S. A. *Plasmonics: Fundamentals and Applications*; Springer Science: New York, 2007.
(10) Wiley, B. J.; Lipomi, D. J.; Bao, J. M.; Capasso, F.; Whitesides, G. M. *Nano Lett.* **2008**, *8*, 3023–3028.
(11) Ditlbacher, H.; Hohenau, A.; Wagner, D.; Kreibig, U.; Rogers, M.; Hofer, F.; Aussenegg, F. R.; Krenn, J. R. *Phys. Rev. Lett.* **2005**, *95*, 4.
(12) Hu, M.; Chen, J. Y.; Marquez, M.; Xia, Y. N.; Hartland, G. V. *J. Phys. Chem. C* **2007**, *111*, 12558–12565.
(13) Jin, R. C.; Jureller, J. E.; Kim, H. Y.; Scherer, N. F. *J. Am. Chem. Soc.* **2005**, *127*, 12482–12483.
(14) Nehl, C. L.; Grady, N. K.; Goodrich, G. P.; Tam, F.; Halas, N. J.; Hafner, J. H. *Nano Lett.* **2004**, *4*, 2355–2359.
(15) Billaud, P.; Marhaba, S.; Cottancin, E.; Arnaud, L.; Bachelier, G.; Bonnet, C.; Del Fatti, N.; Lerme, J.; Vallee, F.; Vialle, J. L.; Broyer, M.; Pellarin, M. *J. Phys. Chem. C* **2008**, *112*, 978–982.
(16) Novo, C.; Funston, A. M.; Pastoriza-Santos, I.; Liz-Marzan, L. M.; Mulvaney, P. *Angew. Chem., Int. Ed.* **2007**, *46*, 3517–3520.
(17) Quinten, M.; Leitner, A.; Krenn, J. R.; Aussenegg, F. R. *Opt. Lett.* **1998**, *23*, 1331–1333.
(18) Harris, N.; Arnold, M. D.; Blaber, M. G.; Ford, M. J. *J. Phys. Chem. C* **2009**, *113*, 2784–2791.
(19) Fung, K. H.; Chan, C. T. *Opt. Commun.* **2008**, *281*, 855–864.
(20) Koenderink, A. F.; de Waele, R.; Prangsma, J. C.; Polman, A. *Phys. Rev. B* **2007**, *76*, 4.
(21) Brongersma, M. L.; Hartman, J. W.; Atwater, H. A. *Phys. Rev. B* **2000**, *62*, 16356–16359.
(22) Park, S. Y.; Stroud, D. *Phys. Rev. B* **2004**, *69*, 7.
(23) Zuloaga, J.; Prodan, E.; Nordlander, P. *Nano Lett.* **2009**, *9*, 887–891.
(24) Rodriguez-Fernandez, J.; Perez-Juste, J.; de Abajo, F. J. G.; Liz-Marzan, L. M. *Langmuir* **2006**, *22*, 7007–7010.
(25) Yao, H.; Yi, C. Q.; Tzang, C. H.; Zhu, J. J.; Yang, M. S. *Nanotechnology* **2007**, *18*, 1–7.
(26) Funston, A. M.; Novo, C.; Davis, T. J.; Mulvaney, P. *Nano Lett.* **2009**, *9*, 1651–1658.
(27) Funston, A.; Davis, T. J.; Novo, C.; Mulvaney, P. *Philos. Trans. R. Soc., A* **2011**.
(28) Nordlander, P.; Oubre, C.; Prodan, E.; Li, K.; Stockman, M. I. *Nano Lett.* **2004**, *4*, 899–903.
(29) Prodan, E.; Radloff, C.; Halas, N. J.; Nordlander, P. *Science* **2003**, *302*, 419–422.
(30) Citrin, D. S. *Nano Lett.* **2005**, *5*, 985–989.
(31) Willingham, B.; Link, S. *Opt. Express* **2011**, *19*, 6450–6461.
(32) Ruting, F. *Phys. Rev. B* **2011**, *83*, 5.
(33) Alu, A.; Engheta, N. *New J. Phys.* **2010**, *12*, 14.
(34) Maier, S.; Brongersma, M.; Kik, P.; Atwater, H. *Phys. Rev. B* **2002**, *65*, 193408–193408.
(35) Koenderink, A. F.; Polman, A. *Phys. Rev. B* **2006**, *74*, 4.
(36) Davis, T. J.; Gomez, D. E.; Vernon, K. C. *Nano Lett.* **2010**, *10*, 2618–2625.
(37) Davis, T. J.; Vernon, K. C.; Gomez, D. E. *Phys. Rev. B* **2009**, *79*, 10.

(38) Gomez, D. E.; Vernon, K. C.; Davis, T. J. *Phys. Rev. B* **2010**, *81*, 10.
(39) Starzak, M. *Mathematical methods in chemistry and physics*; Plenum Publishing Corporation: New York, 1989.
(40) Novo, C.; Funston, A. M.; Pastoriza-Santos, I.; Liz-Marzan, L. M.; Mulvaney, P. *J. Phys. Chem. C* **2008**, *112*, 3–7.
(41) Lowdin, P. O. *J. Chem. Phys.* **1951**, *19*, 1396–1401.
(42) de Abajo, F. J. G.; Howie, A. *Phys. Rev. Lett.* **1998**, *80*, 5180–5183.
(43) de Abajo, F. J. G.; Howie, A. *Phys. Rev. B* **2002**, *65*, 17.
(44) Vernon, K. C.; Funston, A. M.; Novo, C.; Gomez, D. E.; Mulvaney, P.; Davis, T. J. *Nano Lett.* **2010**, *10*, 2080–2086.
(45) Knight, M. W.; Wu, Y. P.; Lassiter, J. B.; Nordlander, P.; Halas, N. J. *Nano Lett.* **2009**, *9*, 2188–2192.